International Journal of Current Engineering and Technology
E-ISSN 2277 – 4106, P-ISSN 2347 – 5161

Available at http://inpressco.com/category/ijcet

Research Article

Numerical Investigation on the Crater Geometry in Abrasive Water Jet Turning Process

Y. Abdelhameed*, A. I. Hassan and Saleh Kaytbay

Mechanical Engineering Department, Benha Faculty of Engineering, Benha University, Egypt

Received 02 July 2019, Accepted 03 Sept 2019, Available online 06 Sept 2019, **Vol.9, No.5 (Sept/Oct 2019)**

Abstract

Abrasive water jet turning (AWJT) is an advanced machining technique surpassing the traditional turning by not inducing severe thermal or mechanical stresses in the machining zone. Nevertheless, controlling the performance of this process is very challenging as being dominated by several process parameters in addition to the complex physical nature of material removal. The present work aims to create a finite element (FE) model in order to examine the effect of traverse rate and jet impact angle on the erosion process in the radial mode of AWJT. The chosen workpiece material was AISI 4340 and the material model of Johnson-Cook (JC) was adopted for it to realize its behavior. The 3^2 full factorial design was employed to prepare the test plan under three levels of the two process factors. After performing the simulations, the crater geometry was observed for each factor combination in the test plan. The model results were consistent to some extent with the experimental studies and can be further used to predict the radial depth of cut (DOC) in AWJT.

Keywords: *Abrasive Water Jet Turning, Finite Element Analysis, Crater Geometry, Multiple Particle Impacts.*

1. Introduction

Turning operations can be conducted on an ordinary abrasive water jet (AWJ) machine using an additional device (turning fixture) mounted on the machine bed. This fixture is used for holding the rotating workpiece while feeding the cutting nozzle parallel to the rotation axis over the workpiece surface. Thus, the material is removed from the workpiece surface because of the erosion process where the final depth of cut (DOC) results from the overlapped jet footprints. Fig.1 shows the radial-mode of abrasive water jet turning (AWJT) in which the nozzle is allowed to be tilted while being fed above and along the central axis of the workpiece. The direct estimation of final DOC in this mode is very difficult as the cutting tool (AWJ) geometry is not fixed. Therefore, further work has to be carried out so as to explore and analyze the effect of process factors on the erosion process.

In AWJT, the final obtained DOC is influenced by several parameters like the water jet pressure, traverse rate, abrasive flow rate, workpiece rotational speed, and jet impact angle. Li *et al*. (2012) conducted an experimental investigation to explore the influence of such process factors on the radial DOC while turning AISI 4340. It was demonstrated that both the water jet pressure and traverse rate are the most significant factors affecting the DOC.

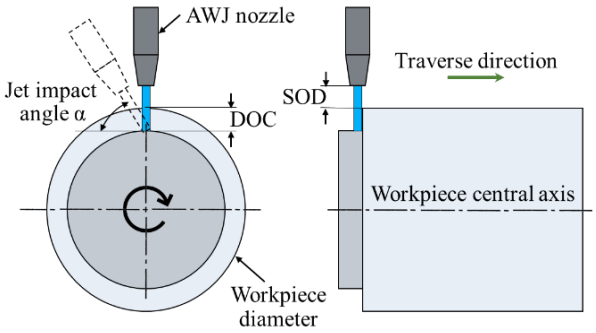

Fig.1 Radial-mode of abrasive water jet turning

It was also shown that the DOC decreases while increasing the traverse rate while being slightly dependent on the jet impact angle. The same authors Li *et al*. (2013), extended their work and developed an empirical model to predict the DOC by using the dimensional analysis technique. This model was evaluated under four levels of water jet pressure, traverse rate, abrasive flow rate, workpiece surface speed, and jet impact angle. The mean error between the predictions and experimental results was 0.2%.

Regarding the finite element analysis (FEA), it was frequently utilized to analyze the crater shape resulting from either the single or multiple abrasive impacts in AWJ machining. Junkar *et al*. (2006) created a finite element (FE) model to observe the crater sphericity due to the single-particle impact on AISI 304 workpiece.

*Corresponding author's ORCID ID: 0000-0002-4927-207X
DOI: https://doi.org/10.14741/ijcet/v.9.5.1

The impacting abrasive particle was modeled as a rigid spherical body while the workpiece was modeled with an elastic-plastic model. After analyzing the crater sphericity at different impact velocities and angles, it was found that increasing the impact angle would increase the sphericity. On the other hand, the crater sphericity was slightly affected by the impact velocity of the abrasive particle. Anwar *et al*. (2011) developed another model to investigate the effect of impact angle on the crater area under three different values. The workpiece material (Ti–6Al–4V) was realized in the simulation using the Johnson-cook (JC) model whilst the impacting steel particle was modeled as elastic-plastic with a failure criterion. It was shown that the crater area increases while increasing the impact angle. The model predictions were satisfactory and showed a maximum difference of 85% from the corresponding experimental data.

Anwar *et al*. (2013) extended the previous work by analyzing the crater shape in 3D rather than 2D under multiple particle impacts. The newly developed model examined the effect of the water jet pressure, traverse rate, and impacting abrasive mass on the crater profile. For the first time, the consideration of actual shape and size distributions of abrasive particles was introduced while building that model. The behavior of workpiece material (Ti–6Al–4V) was described using the JC model while the abrasives (#80 garnet) were modeled using the tensile failure criterion. The prediction results of this model showed a remarkable agreement with the corresponding experimental data with a mean relative error of less than 10%.

The current paper presents an attempt to extend the previously discussed FE investigations to analyze the crater geometry under multiple impacts in the radial-mode AWJT. Both the traverse rate and jet impact angle were the two considered parameters in the numerical simulation while maintaining the other factors fixed. The crater geometry was observed under three levels of these two variables while taking into consideration the actual distribution of the abrasive particles.

2. Finite Element Modeling

In the present study, the numerical investigation was conducted by employing similar turning conditions to that used in (Li, *et al,* 2013). The workpiece material was assigned to be alloy steel (AISI 4340) having a diameter of 59 mm while the adopted abrasive type was #80 garnet. The full factorial design (3^2) was used to prepare the investigation plan, and hence, a total of nine factor combinations were taken into account in the numerical study. The turning conditions applied in the present FE model are shown in Table 1.

Table 1 Conditions applied in the present FE model

Parameter	Symbol	Value
Traverse speed (mm/s)	v_f	0.05, 0.1, 0.15
Jet impact angle (deg)	α	60, 75, 90
Water jet pressure (MPa)	P	380
Abrasive flow rate (g/s)	$\dot{m}_a$	7
Surface speed (m/s)	v_s	2.4
Jet diameter (mm)	D_j	0.76

2.2 Material modeling

The JC model (Johnson and Cook, 1983) was employed for modeling the target material due to its reliability in realizing the behavior of ductile materials while being undergone high strain rates. In this material model, the equivalent von Mises plastic stress can be expressed as a function of the strain, strain rate, and temperature according to the following equation:

$$\sigma = [A + B\varepsilon^n]\left[1 + C\, ln\left(\frac{\dot{\varepsilon}}{\dot{\varepsilon}_0}\right)\right]\left[1 - \left(\frac{T - T_r}{T_m - T_r}\right)^m\right] \quad (1)$$

Where σ is the von Mises plastic stress, A is the initial yield strength at reference strain rate, B is the strain hardening modulus, ε is the strain, $\dot{\varepsilon}$ is the strain rate, $\dot{\varepsilon}_0$ is the reference plastic strain rate, n is the strain hardening exponent, C is the coefficient of strain rate sensitivity, m is the thermal softening exponent, T is the absolute temperature, T_r is the room temperature, and T_m is the workpiece melting temperature.

The JC fracture model (Johnson and Cook, 1985) was employed to model the ductile fracture behavior of workpiece material due to the consecutive impacts of the abrasives. According to this model, the equivalent plastic strain at failure is expressed as follows:

$$\varepsilon_f = \left[D_1 + D_2 e^{D_3 \sigma^*}\right]\left[1 + D_4\, ln\left(\frac{\dot{\varepsilon}}{\dot{\varepsilon}_0}\right)\right]\left[1 + D_5\left(\frac{T - T_r}{T_m - T_r}\right)\right] \quad (2)$$

Where ε_f is the equivalent failure strain, σ^* is the ratio of pressure stress to von Mises equivalent stress and D_{1-5} are material coefficients. The damage criterion of this failure model involves the cumulative equivalent plastic strain to describe the damage behavior using the following equation:

$$D = \sum \frac{\Delta\varepsilon}{\varepsilon_f} \quad (3)$$

Where $\Delta\varepsilon$ is the increment of equivalent plastic strain, and D is the damage parameter where the elements of material undergo ductile fracture if the value of this damage parameter exceeds unity.

The JC model constants used for AISI 4340 in the present investigation are listed in Table 2. On the other hand, the tensile failure criterion was involved in order to realize the brittle fracture behavior of the abrasive particles after impacting the workpiece. By employing this criterion, the elements of abrasive particles fail if the cutoff stress (σ_{cutoff}) reaches the value of 150 MPa (Anwar, *et al,* 2013).

Table 2 JC model coefficients of AISI 4340 (Navarro, *et al,* 2018)

Material property	Symbol	Value
Density (kg/m3)	ρ	7830
Elastic modulus (GPa)	E	207
Poisson's ratio	v	0.29
Reference temperature (°K)	T_r	300
Melting temperature (°K)	T_m	1793
Yield strength (MPa)	A	792
Hardening constant (MPa)	B	510
Strain hardening exponent	n	0.26
Strain rate constant	C	0.014
Thermal softening exponent	m	1.03
JC damage parameter	D_1	0.05
JC damage parameter	D_2	3.44
JC damage parameter	D_3	-2.12
JC damage parameter	D_4	0.002
JC damage parameter	D_5	0.61

2.2 Assembly and meshing

A 3D explicit model was created in ABAQUS/CAE to simulate the multiple impacts of the abrasive particles, as shown in Fig.2. The shape used for modeling the workpiece was a cylinder segment and different shapes were selected for the abrasive particles. The aim of this developed model is to analyze the crater geometry at different process factors. This analysis should be done in a region where the erosion rate is almost constant as a result of the largest possible number of interfered impacts. For this reason, the jet was allowed to cover a distance larger than its diameter and equals 0.9 mm to fulfill the previous condition, and so the workpiece was allowed to rotate 1.75° about its central axis.

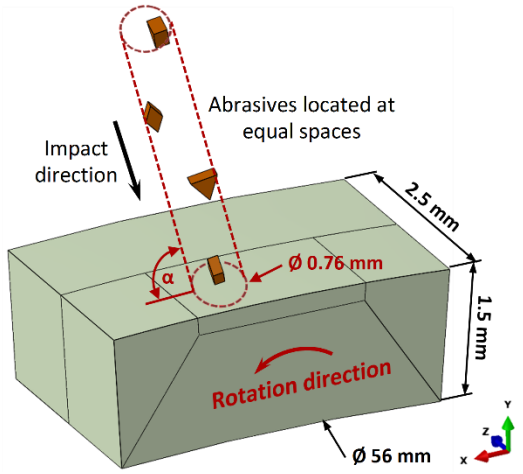

Fig.2 Model assembly

The distance between every two successive particles was the same along the jet axis direction. The actual distribution of the abrasive particles was taken into account by using the same methodology employed by Anwar *et al*. (2013) in order to model these particles within the FE simulation. But first, a series of crucial calculations were carried out. The total abrasive mass was calculated as follows:

$$m_t = 0.82 \frac{d}{1000\, v_s} \dot{m}_a \tag{4}$$

Where m_t is the total mass (g) of abrasive particles, $\dot{m}_a$ is the abrasive flow rate and 82% is the amount of abrasive particles effectively influencing the erosion rate (Anwar, *et al,* 2013). The total number of abrasives was calculated using the following equation:

$$n_p = 19 \frac{m_t}{m_{pm}} \tag{5}$$

Where n_p is the total number of abrasives and m_{pm} is the mass of a particle mix which was calculated to be 0.00021 g. The total length of the jet axis L_j (mm) was obtained with the following equation:

$$L_j = \frac{d}{v_s} v_a \tag{6}$$

Finally, the equal space between every two particles was obtained as follows:

$$S = \frac{L_j}{n_p} \tag{7}$$

A translational motion was applied to the abrasive particles along the jet axis so as to define the impacting velocity of these particles. The velocity magnitude can be determined by employing the following equation (Liu, *et el,* 2016):

$$v_a = 29.52 \sqrt{P} \tag{8}$$

Where v_a is the impacting velocity (m/s) and P is the water jet pressure (MPa).

The workpiece was allowed to translate and rotate with speeds equal the traverse rate and rotation speed, respectively. After performing the previously discussed calculations, the numerical conditions employed in the present study could be listed as shown in Table 3.

Table 3 Numerical conditions used within the present FE model

v_f (m/s)	α (deg)	v_a (m/s)	n_p
0.05, 0.1, 0.15	60, 75, 90	575.5	195
S (mm)	**D_j (mm)**	**N (rad/s)**	**Rot. angle**
1.11	0.76	81.36	1.75°

The mesh size of the workpiece was refined in the impact zone to be 14 × 5 × 14 μm^3 while elements with an edge length of 25 μm were used in the impacting particles, as shown in Fig.3. The type of elements used for all the parts within the FE assembly was 3D stress elements (C3D8R) with hourglass control. The element deletion in ABAQUS was applied to eliminate the failed elements so as to enhance the computational efficiency. The general surface-to-surface contact algorithm was adopted to mimic the interaction between the abrasives and workpiece with a friction coefficient of 0.1.

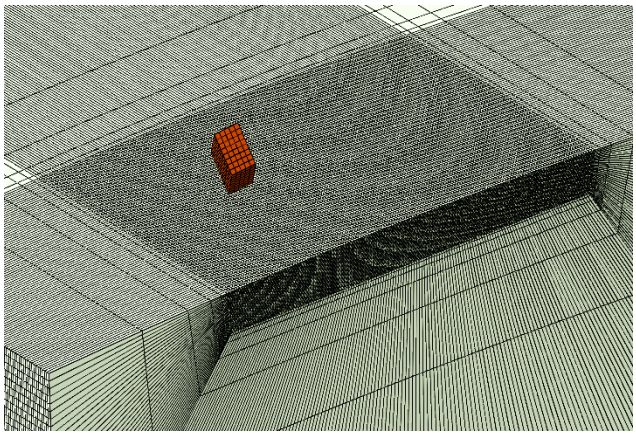

Fig.3 Meshed geometry

3. Results and discussion

Fig.4 illustrates an example of the model results after conducting the simulation. Fig.4(b) shows the obtained crater profile for analysis. This profile can be gotten by using a cutting plane at the middle of the impact zone where the largest number of interfered impacts exists, as demonstrated in Fig.4(a).

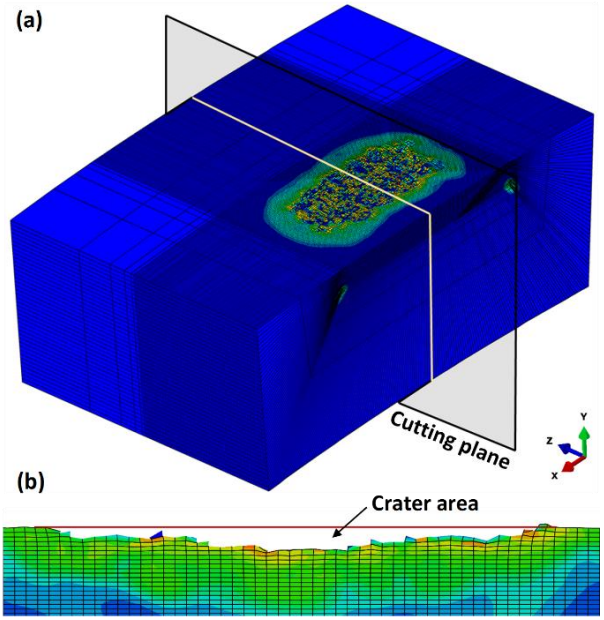

Fig. 4 (a) 3D view of a simulation example. (b) cross sectional side view showing the crater

Fig. 5 illustrates the effect of the traverse rate on the crater area. It can be observed that increasing the traverse rate would decrease the crater area. The trend of decrease is more apparent at lower jet impact angles. This trend was also observed in the experimental data published by Li *et al*. (2013). However, increasing the traverse rate (e.g. at 60°) decreases the experimental DOC by 69.7% while the crater area is only decreased by 6%. This is attributed to the significant effect of the traverse rate on the jet overlapping which significantly affects the experimental DOC. Hence, this effect was not revealed by the present model as the jet overlapping effect was not considered in the current study.

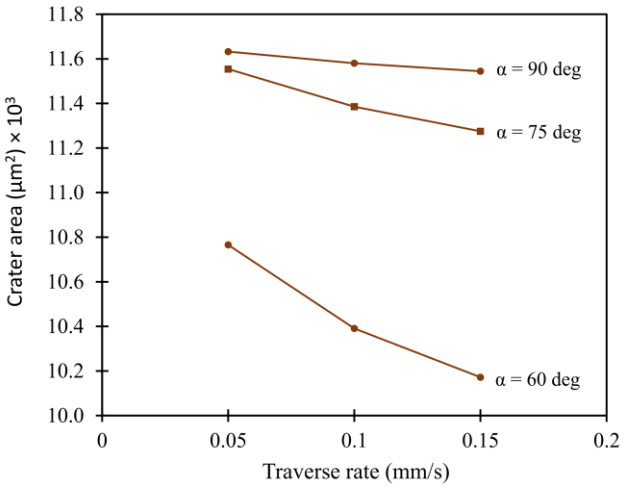

Fig.5 Effect of traverse rate on crater area

Fig. 6 presents the effect of the jet impact angle on the crater area. An increase can be obviously observed in the crater area when increasing the jet impact angle and this increasing rate is gradually decreased at higher angles. It can be deduced that increasing the impact angle from 60° to 90° would increase the crater area by 8% at traverse rate of 0.05 mm/s. A close percentage (10%) in the DOC increase was found while increasing the jet impact angle at the same conditions. Therefore, the current FE model succeeded to closely mimic the effect of the jet impact angle.

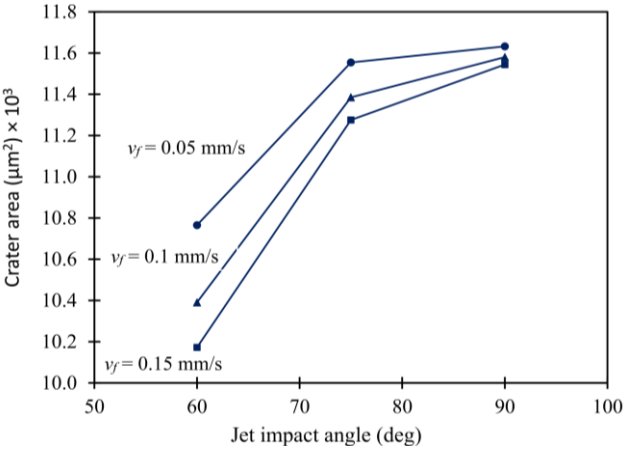

Fig.6 Effect of jet impact angle on crater area

Conclusions

In the present paper, the FEA approach was employed to simulate the multiple impacts in AWJT process while turning AISI 4340. The developed model offers a good extension for the previous studies in investigating the crater geometry. The crater area was observed under three levels of traverse rate and jet impact angle while taking the actual distribution of the abrasive particles into consideration. It was observed that increasing the traverse rate would decrease the crater area. However, the increasing percentage of crater area does not agree with the experimental results. On the other side, it was found that the crater area increases in a similar manner to the experimental results when increasing the impact angle. Therefore, the current model proved its ability to simulate the effect of the jet impact angle.

Examining the influence of process factors on the crater geometry is very beneficial in understanding the AWJT process. Despite that, it is extremely difficult to directly validate the crater geometry by experimental tests where the final obtained DOC from machining is the result of jet overlaps along the traverse direction. Thus, further investigations should be undertaken to develop a methodology for deriving the final numerical DOC. Also, additional work should be carried out to reduce the model errors.

References

W. Y. Li, J. Wang, Y. M. Ali, (2012), An experimental study of radial-mode abrasive waterjet turning of steels, *Materials Science Forum*, 697, 166-170.

W. Li, H. Zhu, J. Wang, Y. M. Ali, C. Huang, (2013), An investigation into the radial-mode abrasive waterjet turning process on high tensile steels, *International Journal of Mechanical Sciences*, 77, 365-376.

M. Junkar, B. Jurisevic, M. Fajdiga, M. Grah, (2006), Finite element analysis of single-particle impact in abrasive water jet machining, *International Journal of Impact Engineering*, 32, 1095-1112.

S. Anwar, D. A. Axinte, A. A. Becker, (2011), Finite element modelling of a single-particle impact during abrasive waterjet milling, *Part J: Journal of Engineering Tribology*, 225, 821-832.

S. Anwar, D. A. Axinte, A. A. Becker, (2013), Finite element modelling of abrasive waterjet milled footprints, *Journal of Materials Processing Technology*, 213, 180-193.

G. R. Johnson, W. H. Cook, (1983), A constitutive model and data for metals subjected to large strains, high strain rates and high temperatures, *International Symposium on Ballistics*, 541-547.

G. R. Johnson, W. H. Cook, (1985), Fracture characteristics of three metals subjected to various strains, strain rates, temperatures and pressures, *Engineering Fracture Mechanics*, 21, 31-48.

P. F. Navarro, P.-H. Chiu, A. Higgins, M. Serge, D. J. Benson, V. F. Nesterenko, (2018), Shear band patterning and post-critical behavior in AISI 4340 steel with different microstructure, *International Journal of Impact Engineering*, 112, 144-154.

D. Liu, H. Zhu, C. Huang, J. Wang, P. Yao, (2016), Prediction model of depth of penetration for alumina ceramics turned by abrasive waterjet-finite element method and experimental study, *The International Journal of Advanced Manufacturing Technology*, 87, 2673-2682.